

Simulating the Joining of Composite Materials by Electromagnetic Induction

M. Duhovic, L. Moser, P. Mitschang, M. Maier

*Institut für Verbundwerkstoffe GmbH, Erwin-Schrödinger-Str., Building 58
67663 Kaiserslautern, Germany*

I. Caldichoury, P. L'Eplattenier

*Livermore Software Technology Corporation, 7374 Las Positas Road, Livermore,
CA 94551, USA*

Abstract

The development of the electromagnetism module in LS-DYNA (980 solver) was in the past primarily driven by the need for Electromagnetic Metal Forming (EMF) simulation capabilities. As the module matures, new applications in particular in the field of induction heating for thermoplastic composite welding/joining have appeared, providing a crucial simulation tool for composite manufacturing processes utilizing this technology. In this work, induction heating characterization tests involving static plate specimens using different induction heating processing parameters have been performed and then simulated. Finite element models have been built in both LS-DYNA and COMSOL and the results and capabilities of both software codes are discussed and compared.

1-Introduction

The push by automotive manufacturers towards the mass production of all carbon fiber composite passenger cells like that in BMW's fully electric mega city vehicle (i3) and its hybrid sports counterpart the i8, together with Volkswagen Group (Lamborghini) and GM among others all considering the wider use of composite materials, calls for more automated production methods for automotive composites. Currently, such passenger cells (Figure 1) are produced using "semi-automated" resin transfer molding (RTM) processing techniques that still require a significant amount of manual labor. On the material cost side, vigorous research efforts are underway to find out ways of producing cheaper higher quality carbon fiber materials indicating again a clear trend towards the increasing use of these types of materials. Beyond the concept cars of today, the mass production of carbon fiber thermoplastic composite parts for vehicles can be foreseen in the future considering the lightweight and customizable performance advantages that can be offered. Thermoplastic composite sheet materials have already demonstrated their potential in quick thermoforming processing techniques which are not so far away in principle from the stamping processes currently performed during automotive sheet metal part manufacturing.

An important part of the vehicle body construction is welding and joining. Joining methods for metallic passenger cells and chassis components include automated robotic spot and seam

welding of pre-stamped parts along with glueing in some areas mainly for providing water sealing properties. For the use of thermoplastic carbon fiber parts to therefore become feasible for automotive mass production one very important characteristic is therefore required; the ability for the material to be joined quickly and efficiently by robotic means in a controlled manner to give excellent bonding between the connected parts.

The technology to provide this capability for both metal to composite and composite to composite thermoplastic parts has been in development at the Institute für Verbundwerkstoffe (IVW) over the last 15 years, in the form of robotic composite induction welding, see Figure 1. Early methods focused on the use of susceptor materials (a metallic mesh) inserted between the laminates so that a concentrated heating effect could be generated at the bond line. However, it is now known that in woven carbon fiber reinforcement structures, eddy current joule heating can produce enough heat in the composite to allow for thermal bonding to occur without the use of susceptors. With the correct selection of electromagnetic, thermal and mechanical parameters the composite can be melted precisely in a small volume of material close to the bond line so that the two parts can be joined effectively without any detrimental effects of overheating and deconsolidation. Figure 1 (right) shows the robotic induction welding of a BMW M-series front bumper beam using a Kuka robot fitted with an induction heating head incorporating a coil and roller pressure system.



Figure 1: Examples of automotive components that could or have already benefitted from induction welding (left). Induction welding Kuka robot at the Institute für Verbundwerkstoffe (right) joining the two thermoformed components of the BMW M-series front bumper beam

At present, the selection of the optimum processing parameters for the induction welding of composites is an art form only known by a handful of researchers who have spent many hours operating the equipment and burning thousands of dollars of expensive test material in the process (2 mm thick CF/PEEK (Carbon fiber reinforced polyether ether ketone composite))

organosheet material costs $\sim 200 \text{ €/m}^2$). While the trial and error method may give some result in the end, an understanding of how to control the induction welding process properly in order to create defect free bonding between the thermoformed parts still remains a mystery. In addition, the selection of a new material results in a completely different set of processing parameters. It is for these reasons that strong developments in the field of finite element simulation of such processing techniques are currently being developed.

The simulation of material processing using electromagnetic induction is a multiphysics problem involving at least the theories of electromagnetism and heat transfer. If the thermal and mechanical stresses are also to be taken into account then a three-way Electro-Thermal-Mechanical (ETM) simulation coupling is required. Two Finite Element Analysis (FEA) software codes capable of such simulations are COMSOL AB's COMSOL Multiphysics and LSTC's LS-DYNA 980 solver. For the simulation of induction heating problems COMSOL Multiphysics uses a complete finite element method formulation. This means that all the domains (including the coil, conducting and non-conducting workpiece parts) and the surrounding air are represented by solid 3D elements. The LS-DYNA 980 alpha solver on the other hand uses a combination of the boundary element (BEM) and finite element (FEM) methods. In this case, the electromagnetic behavior is accounted for by boundary elements coupled to the outer surfaces of the parts meshed using solid 3D finite elements which take care of the model's thermal and mechanical behavior. There are advantages and disadvantages with both methods. The former, for example, provides a more efficient formulation for large static induction heating simulations while the latter is more suited for smaller dynamic simulations where a moving coil or workpiece is required. For very large models the BEM method requires a significant amount of memory for the storage of the system matrices. However, the disadvantage of using the full FEM method is that any model considering anything but simple translational movement of the coil geometry requires automated remeshing of the entire model. In the BEM method, no mesh at all is required for the air domain giving rise to the possibility of dynamic transient induction heating simulations (i.e. allowing for a moving coil and workpiece). In addition, for induction heating cases where the coil remains static and workpiece deflection can be neglected, the large system of matrices need only be solved once.

In this work, both FEA codes have been used in order to simulate static induction heating of ordinary steel plate and composite laminates. The characterization experiments necessary for gathering the data for such simulations involve the static heating of plates using different coupling distances, coil geometries and variable induction generator settings (e.g. power, current, voltage and frequency). Two different induction heating characterization tests, involving single steel plate specimens $100 \times 100 \times 0.8 \text{ mm}$ in size, and composite plate specimens $100 \times 100 \times 2.1 \text{ mm}$ in size were performed. Temperature measurements were recorded using laser guided non-contact pyrometers on both sides of the specimens at specific locations depending on the coil geometry. In addition, full infrared thermal imagery was recorded for one side of the specimen setup. The overall temperature information was captured at sampling rate of 50Hz for both the heating and cooling cycles.

2-Experimental equipment

2-1 Induction generator and temperature data recording devices

A Hüttinger Elektronik TruHeat HF 5010 generator available at the IVW, see Figure 2, was used together with an 8:1 transformer unit. The transformer itself contains two sets of interchangeable capacitor slots allowing for a reasonable variation of frequency. It must be noted that for different test setups (coil geometry, heated material type, thickness, coupling distance, etc) the capacitor set used to give a desired range of induction parameters will be different. This is due to the fact that all of the aforementioned parameters are involved in determining the electromagnetic circuit created during induction welding. However, since the coil size and geometry are a major influence, a rough idea of the capacitor set required can be obtained by trialing the coils in the absence of any test specimen.

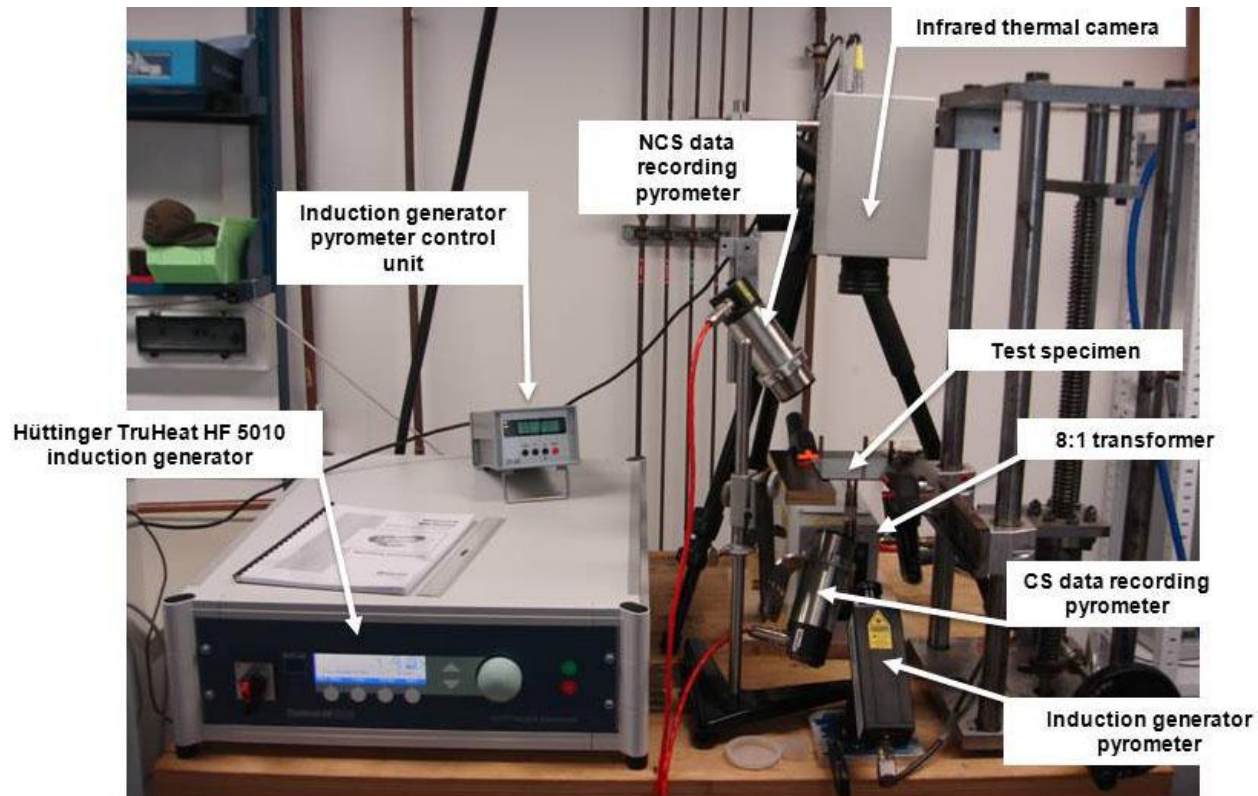


Figure 2: Induction heating characterization equipment at the Institute für Verbundwerkstoffe GmbH

In total, three pyrometers were used during the experiments, one to control the induction generator and two others to take point temperature measurements at defined locations on the coil side (CS) and non-coil side (NCS) of the test specimens. An infrared thermal camera provided full surface temperature data for the NCS of the specimens which in the shown configuration is the top side of the plate specimen. In the test setup shown in Figure 2 the coil (obstructed by the

test specimen in this case) is connected to the transformer and faces the bottom side of the laminate.

2-2 Coil and flux concentrator geometries

Only one coil geometry was chosen for these experiments as presented in Figure 3. The “*pancake*” type spiral induction coil, consists of a tubular cross-section with a 3 mm outer diameter, 0.5 mm wall thickness and an overall spiral diameter of approximately 25 mm. The mesh geometry when created for LS-DYNA consists only of solid hexahedral elements (tetrahedral elements are currently unavailable but are planned in the future) and three coil section surface segment sets are used to define the input, output and flow direction of the applied current. Although complete solid element models are not always necessary to model induction heating, (i.e. we are usually not so interested in the temperature development in the coil itself) the coil mesh geometry developed here for LS-DYNA allows for an investigation of the heat developed in the coil itself. As part of the coil design process, the convective heat transfer coefficient required on the inner surfaces of the coil to keep the coil at a safe temperature can be determined. The appropriate cooling water flow rate can then also be calculated although no further details will be given here. The coil geometry considered here represents only one of the virtually unlimited possibilities available with respect to coil design in order to achieve the desired heating pattern on the workpiece.

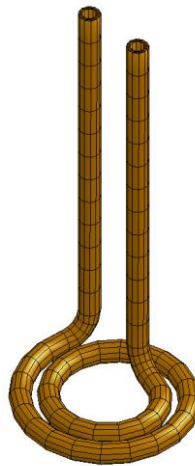


Figure 3: LS-DYNA coil mesh for a “*pancake*” type spiral induction heating coil geometry

3-Characterization tests

For the characterization tests, a single point temperature profile with respect to time was recorded using either two pyrometers on the CS and NCS of the laminate at a defined location (point 4) as indicated to the right of Figure 4. Temperature measurements at points 1, 2 and 3 were obtained using the data recorded from infrared thermal images. The induction generator settings used for the pancake coil were $f = 400$ kHz and three different values of power corresponding to a coil current of $I = 131.97$ A (10% max power), $I = 193.50$ A (20% max

power) and $I = 241.54$ A (30% max power) were applied. A coil coupling distance of 2 mm was maintained for the coil during all the tests performed. A schematic of the induction heating characterization test setup is shown in Figure 4.

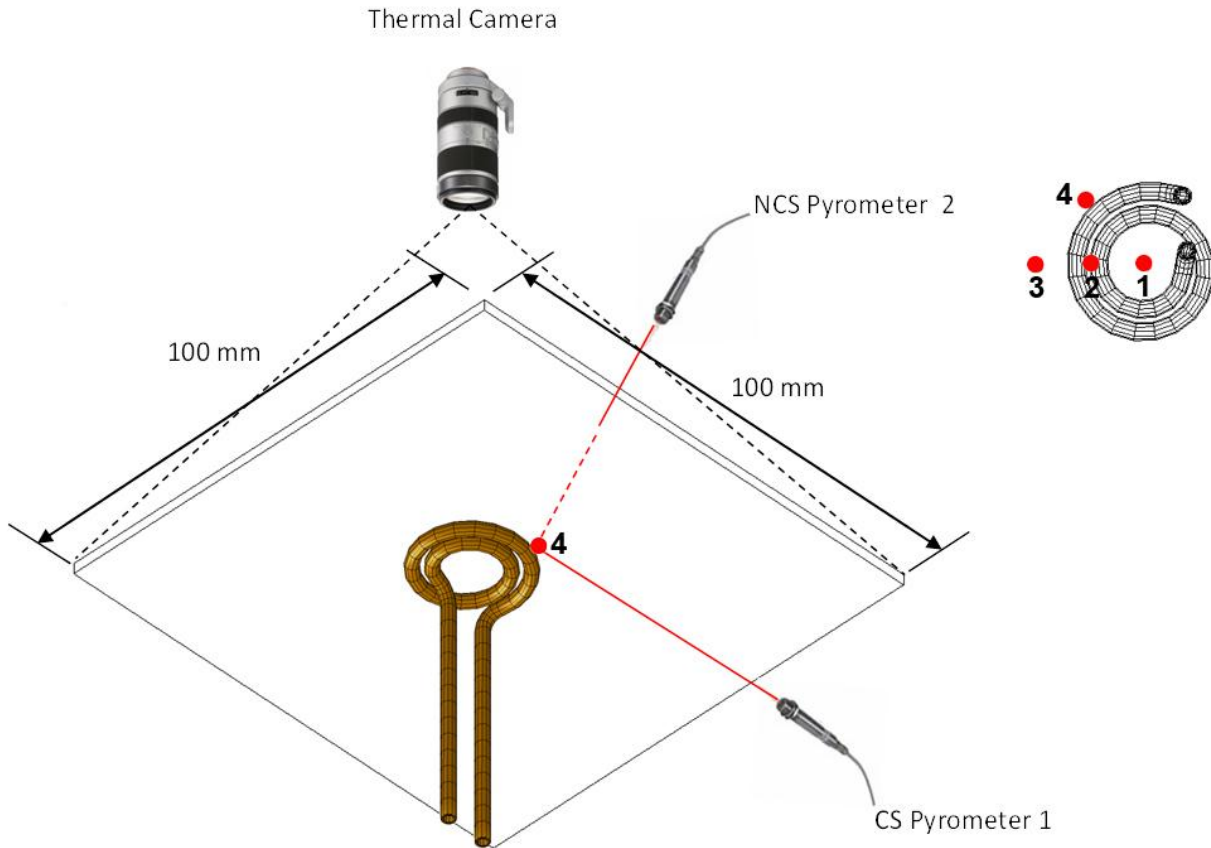


Figure 4: Schematic of test setup for static induction heating characterization and temperature spot measurement locations using the “pancake” type induction heating coil

4-Finite element models

4-1 The inductive heating solver in LS-DYNA

The Electromagnetism (EM) solver included in the 980 version of LS-DYNA solves the Maxwell equations in the Eddy current (induction-diffusion) approximation [1-3]. This is suitable for cases where the propagation of electromagnetic waves in air (or vacuum) can be considered as instantaneous which is the case in most industrial magnetic metal welding, forming or inductive heating applications. The EM solver is coupled with the structural mechanics solver (the Lorentz forces are added to the mechanics equations of motion), and with the structural thermal solver (the Ohmic heating is added to the thermal solver as an extra source of heat) thus allowing the simulation of moving coils and the heating or deformation of work pieces. The EM fields are solved using a Finite Element Method (FEM) for the conductors and a Boundary Element Method (BEM) for the surrounding air/insulators. Thus no air mesh is necessary.

Among its various features, the EM solver in LS-DYNA includes an inductive heating solver. It was introduced in order to solve the computer cost issue arising when high frequency currents, thus very small time steps, were combined with long simulation runs (typically, an AC current with a frequency ranging from kHz to MHz and a total time for the process in the order of a few seconds). The induction heating solver works the following way: it assumes a current which oscillates very rapidly compared to the total time of the process. The following assumption is made: a full eddy-current problem is solved over two full periods with a "micro" EM time step, see Figure 5.

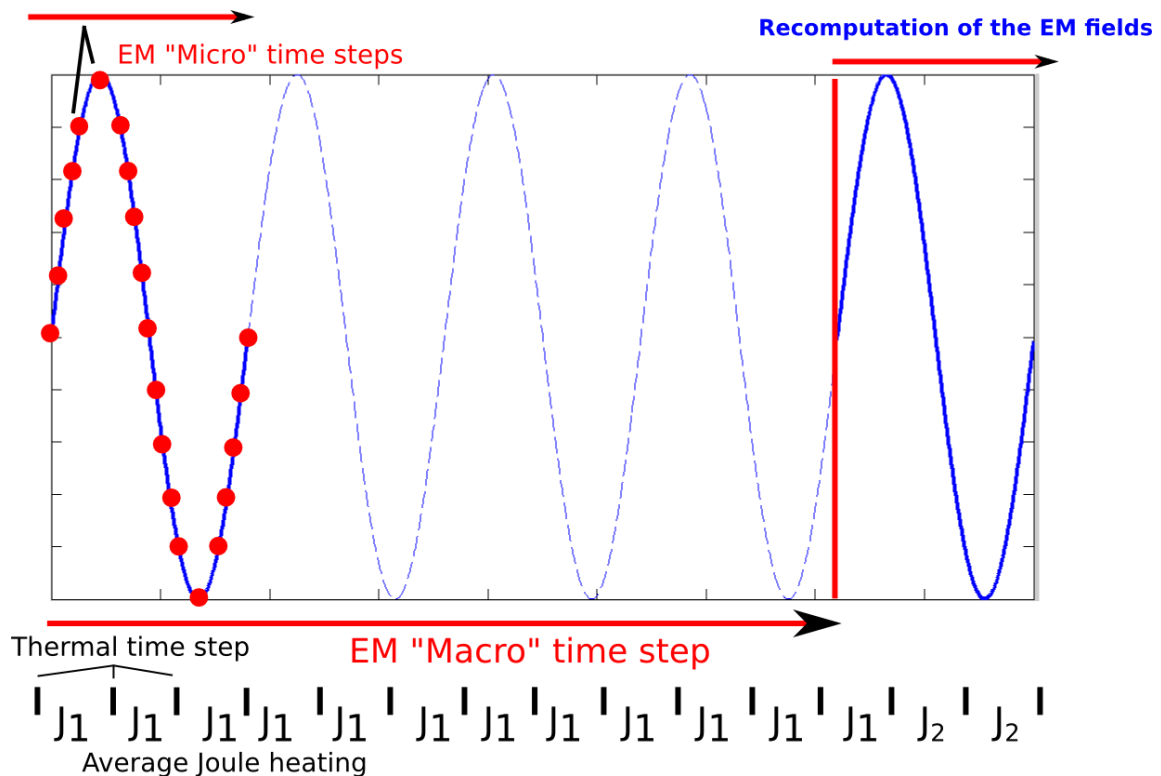


Figure 5: Graphical representation of the electromagnetic field and resulting joule heating calculation scheme implemented in the LS-DYNA inductive heating solver

An average of the EM fields during the two full periods as well as the joule heating is computed. It is then assumed that the properties of the material (heat capacity, thermal conductivity, magnetic permeability) and mostly the electrical conductivity which drives the flow of the current and the joule heating do not change for the next periods of the current within the "macro" EM time step chosen. As all the properties are largely temperature dependent, the assumption can therefore be considered accurate as long as the temperature does not change too much. During these periods, no EM computation is performed; only the averaged joule heating term is added to the thermal solver. However, as the temperature and thus the electrical conductivity changes together with all the other material properties mentioned, the EM fields need to be updated accordingly so another full eddy current resolution is computed for two full periods of the current giving new averaged EM fields (introducing a "macro" EM time step). In this way the solver can efficiently solve inductive heating problems for both the cases of a static

or moving coil. It is also worth noting that velocity of the coil is not a factor with respect to the computational efficiency. For example, a fast moving coil will require the same number of macro time steps to ensure an accurate solution as a slow moving coil. The important parameter in the moving case is therefore the total coil travel distance which is simulated.

4-2 Material properties

A large number of material properties need to be collected in order to setup the simulations. A summary of the properties used in both the LS-DYNA and COMSOL finite element models along with their relevant references are presented in Table 1.

Table 1: Summary of the material property parameters used in the LS-DYNA and COMSOL induction heating finite element models. COMSOL values used are given in brackets if different

Material Property	Air	Coil (Copper)	Steel Plate (0.9% Carbon Structural Steel)	Composite Plate (CF/PEEK)	
Density, ρ (kg/m ³)	1.293 (1.217)	8960	7850	1790	
Heat Capacity at (const. pressure), C_p (J/(kg*K))	1010 (1006)	385	¹ 475 Cp vs. T curve	⁵ 1803 Cp vs. T curve	
Thermal Conductivity, k (W/m*K)	k_1	0.026 (0.025)	390	² 44.5 k vs. T curve	⁶ 2.50
	k_2	-	-	-	⁶ 2.50
	k_3	-	-	-	⁶ 0.32
Electrical Conductivity, σ (S/m)	1	5.998×10^7	³ 1.032×10^6 σ vs. T curve	⁷ 1.389×10^4 σ vs. T curve	
Relative Permittivity, ϵ_r	1	1	1	⁸ 3.7	
Relative Permeability, μ_r	1	1	⁴ 150 B vs. H curve μ_r vs. T curve	1	
Surface Emissivity	-	0.5	(0.95)	(0.95)	
Skin Depth (mm) (automatically calculated)	-	~ 0.1	See Eq. 1	See Eq. 1	

¹Specific heat capacity at room temperature for low carbon structural steel is shown, however from references [4,5] curves defining the property with respect to temperature have been implemented in both the LS-DYNA and COMSOL models.

²Isotropic thermal conductivity at room temperature shown, however from references [4,5] curves defining the property with respect to temperature have been implemented in both the LS-DYNA and COMSOL models.

³Electrical conductivity for AC current source at room temperature for low carbon structural steel shown, however from reference [6] a curve defining the property with respect to temperature has been implemented in both the LS-DYNA and COMSOL models.

⁴Relative permeability value at room temperature for low carbon structural steel shown and used although B vs. H curves where B is the magnetic flux density, H is magnetic field density and μ_r vs. T curves can be defined as given in references [7, 8].

⁵Best constant value over the processing temperature for heat capacity is shown although a curve defining the property with respect to temperature experimentally measured using DSC equipment at IVW has been implemented in both the LS-DYNA and COMSOL models.

^{6,7,8} Values taken from the measurements and data collected in reference [9], thermal conductivity is so low there is no point defining it with respect to temperature in this case.

In the both the LS-DYNA and COMSOL models, the free convection heat transfer coefficients were calculated for the upper, lower and sides faces of the plate. Tabulated values with respect to temperature (for a range of 40 – 480 °C) were input into the models as curves defining the respective convection boundary condition. The average values were 7.83 W/(m².K) for the horizontal upside surface, 5.94 W/(m².K) for the horizontal downside surface and 33.00 W/(m².K) for the vertical faces.

The skin depth is another important electromagnetic parameter where the magnetic field has decreased by a factor of “e” compared to its value at the surface. In LS-DYNA and in COMSOL, it is automatically calculated using the formula given in Equation (1), which is a function of the already specified electromagnetic material properties.

$$\delta = \sqrt{\frac{2\rho}{(2\pi f)(\mu_o\mu_r)}} \approx 503 \sqrt{\frac{\rho}{\mu_r f}} \quad (1)$$

where

δ = the skin depth in meters (calculated using Eq. 1 as 3.5 mm for pancake coil (400

kHz) and 2.85 mm for the single turn coil (600 kHz) for CF/PEEK)

μ_r = the relative permeability of the medium (3.7 used for CF/PEEK, reference [6])

μ_o = the magnetic permeability of free space ($4 \cdot \pi \cdot 10^{-7}$ H/m)

ρ = the resistivity of the medium in $\Omega \cdot m$, also equal to the reciprocal of its conductivity:

$\rho = 1 / \sigma$ (for CF/PEEK, $\rho = 7.14 \times 10^{-5} \Omega \cdot m$, reference [6])

f = the frequency of the current in Hz

4-3 Simulation results and comparisons with Experiments/LS-DYNA/COMSOL

One coil geometry and two different plate material types with large differences in electrical conductivity (structural steel and CF/PEEK polymer composite) have been chosen for these experiments as has been highlighted in the previous sections. The experimental data has then been compared with analyses performed in both LS-DYNA and COMSOL.

4-3-1 Structural steel plate

In the first instance, multiple point in-plane temperature measurements were carried out on the coil side of the steel plate using the pancake type induction coil. The three measurement location points (1, 2 and 3) beginning from the centre of the coil, were chosen in order to demonstrate the in-plane non-uniformity of the developed heating pattern. Measurement location point 4 has not been used for the steel plate experiments but was later arbitrarily chosen to gather the point temperature measurement data on both sides of the thicker composite plate specimen.

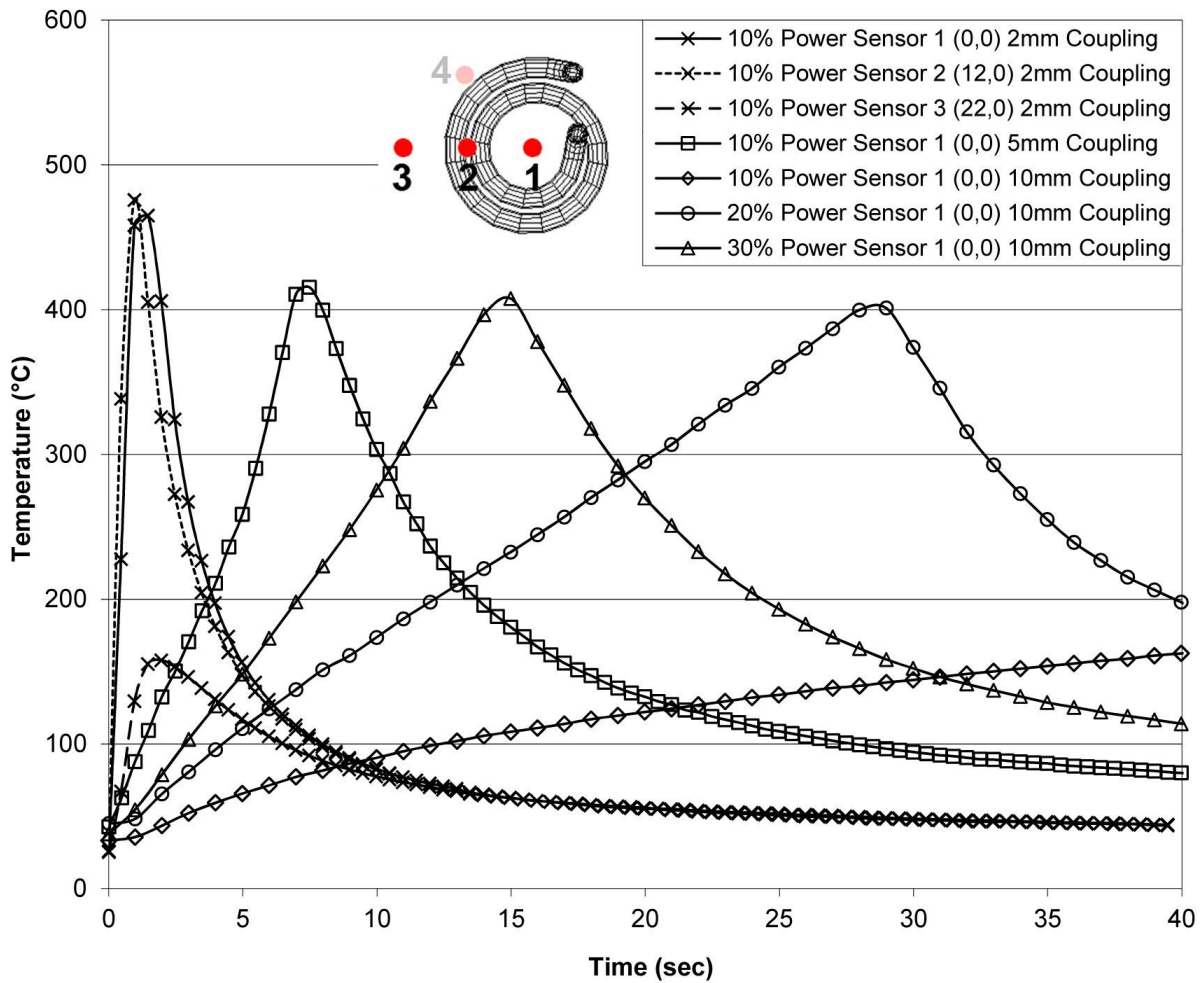


Figure 6: Experimental coil-side surface point temperature measurement curves for a structural steel plate at various power levels 10% (131.97A), 20% (193.5 A), 30% (241.54 A) and coupling distances of 2, 5 and 10 mm, frequency 400 kHz.

As the steel plate used in the experiments was only 0.8 mm thick, there was no detectable difference in the temperatures at the measurement points on the coil and non-coil side of the plate. The experimental point temperature measurement curves are presented in Figure 6. The significance of the induction generator power level (or applied current to the coil) and the value of the coil to plate coupling distance on the heating behaviour can be seen by examining the curves. Each of the curves represents a constant power level of induction heating until a certain target temperature has been reached (in this case approximately 400°C) after which only natural convective cooling takes place. The nature of the heating pattern can be better visualized by looking at infrared thermal images of the heating behavior as shown in Figure 7.

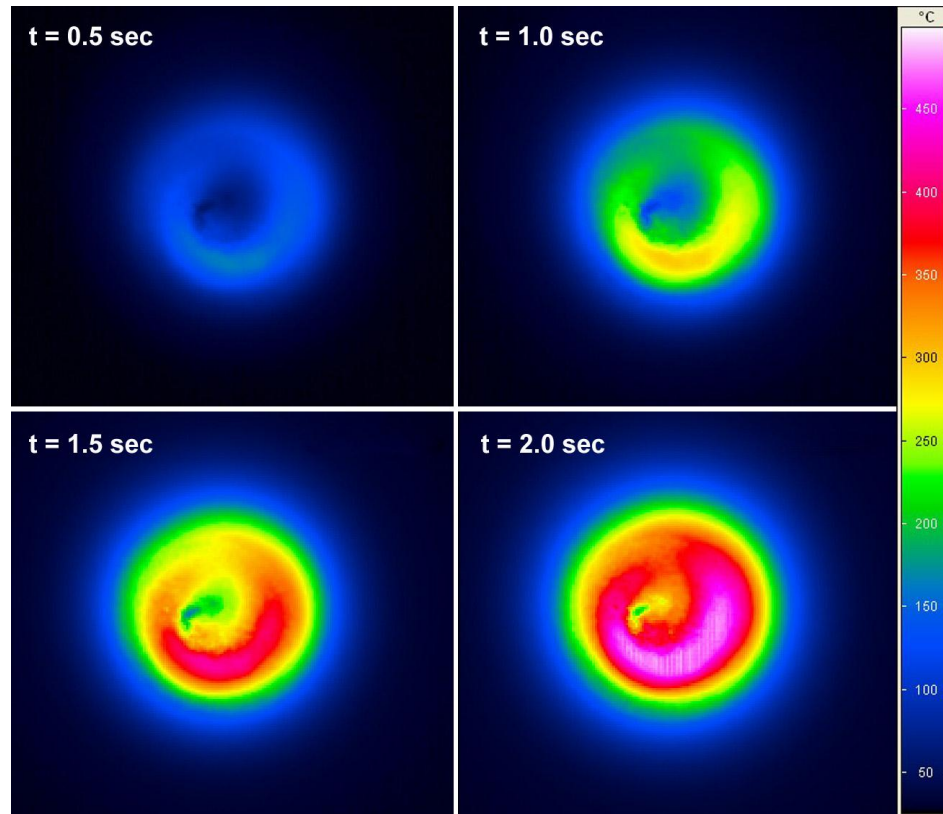


Figure 7: Infrared thermal images showing the experimental surface temperature development on the non-coil side of a 0.8mm thick steel plate for 10% (131.97 A) generator power, 400 kHz and a 2 mm coupling distance.

These experimental results can be compared directly with those predicted by both LS-DYNA and COMSOL. In Figure 8 an equivalent plot for the steel plate measurement points is given showing the results obtained from both software. Note that the convective cooling part of the COMSOL simulation curves has been omitted for clarity and that the heating curves in these cases end at specified values of time (e.g. 2, 10 and 30 sec looking at the curves from left to right). For the same parameter set used experimentally (Figure 6) the plot shows that both LS-DYNA and COMSOL agree well with one another considering the differences which exist in the meshing (LS-DYNA uses hexahedral while COMSOL uses tetrahedral solid elements). It can also be seen that the curves predict the experimental results quite well considering the wide range of material properties which have been defined. Some further detailed features of the experimental curves, for example an increasing slope exhibited by some of the curves can be explained by thermal expansion. The thermal expansion of the thin steel plate causes the coil-side surface of the specimen to move closer to the coil itself therefore reducing the coupling distance. This phenomenon could also be accounted for in LS-DYNA at the expense of computing time. The electromagnetic field would have to be recalculated at a suitable time step in order to capture the dynamics of the thermal expansion giving rise to a changing coupling distance.

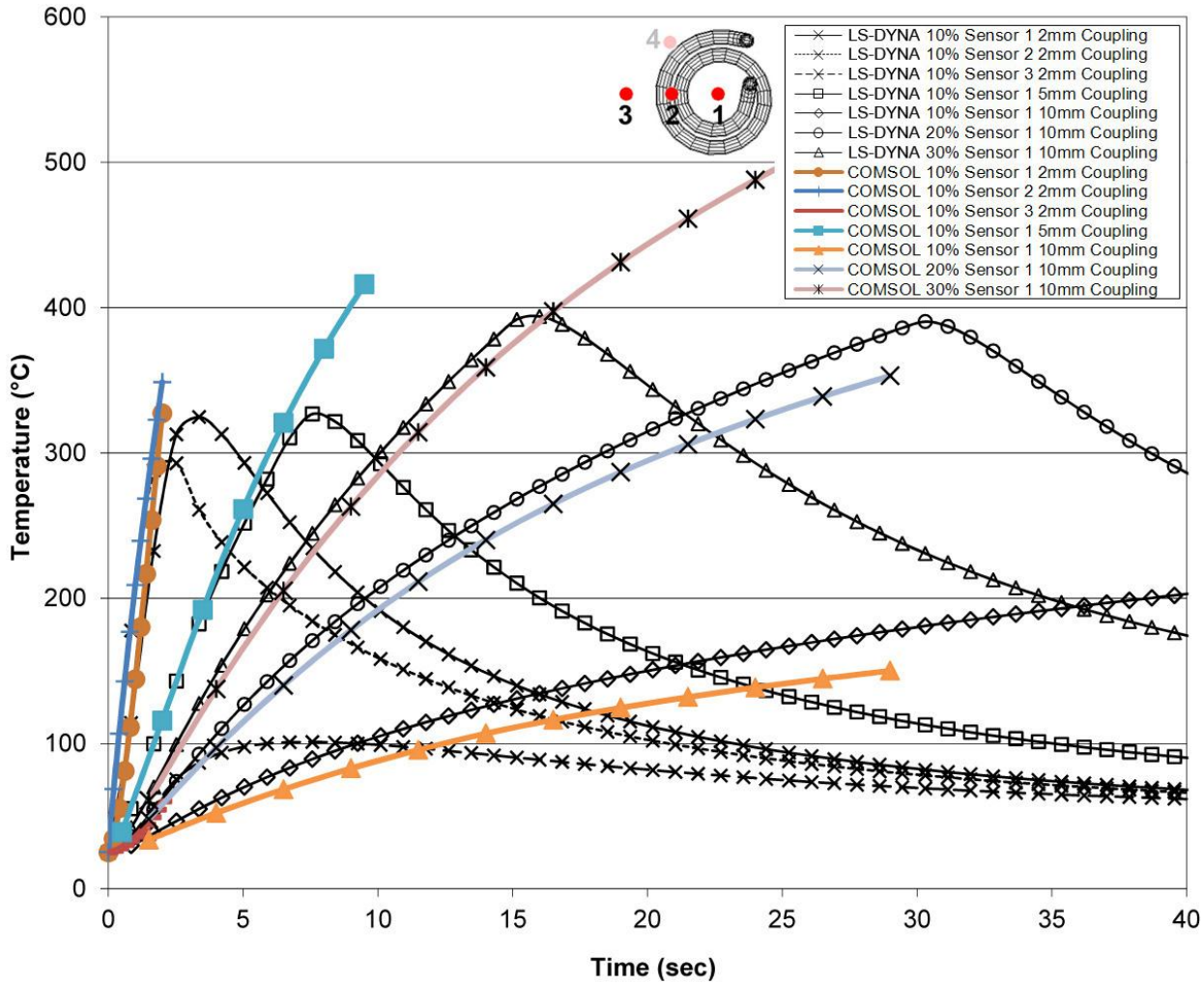


Figure 8: LS-DYNA and COMSOL predicted point temperature curves for a structural steel plate at various power levels 10% (131.97A), 20% (193.5 A), 30% (241.54 A) and coupling distances 2, 5 and 10 mm, frequency 400 kHz.

A comparison of the thermal contour plots obtained from both FEA software codes is shown in Figures 9 a) and b) for the case of 10% power and a coupling distance of 2 mm at a frequency of 400 kHz. This case of rapid heating is the most difficult to model, in particular with a material with high conductivity due to the fast changing temperature field that results. While the nature of the heating pattern is well predicted by both software codes, it can be seen from the heating pattern itself why actual point temperature predictions are very difficult to replicate. Mesh convergence in high conductivity materials due to very small skin depths is another factor which can cause maximum temperature inaccuracies and is discussed in more detail in Section 5.

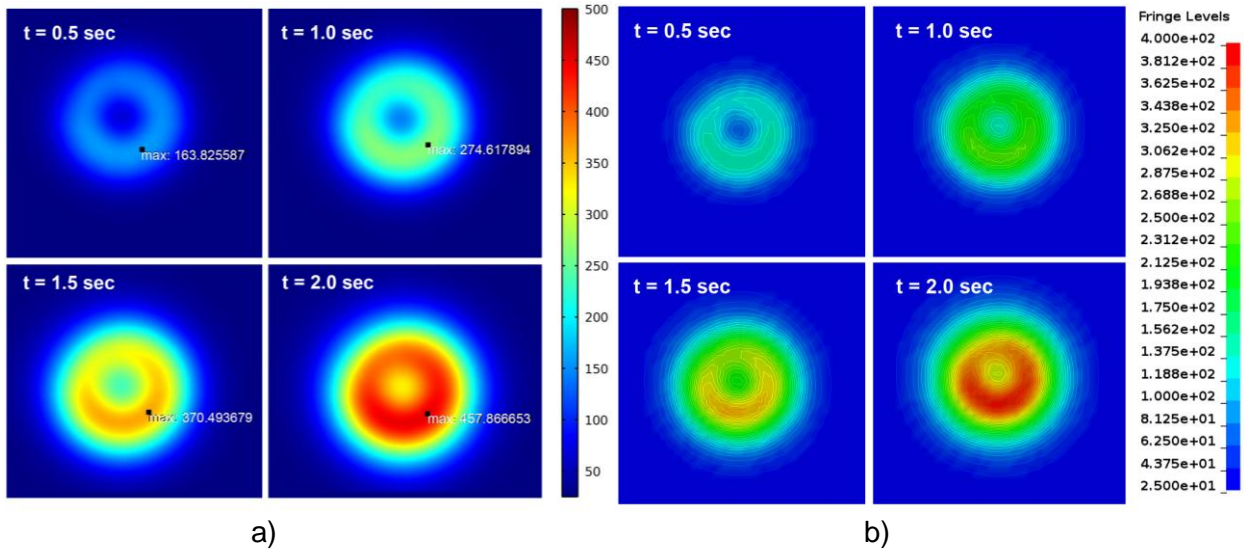
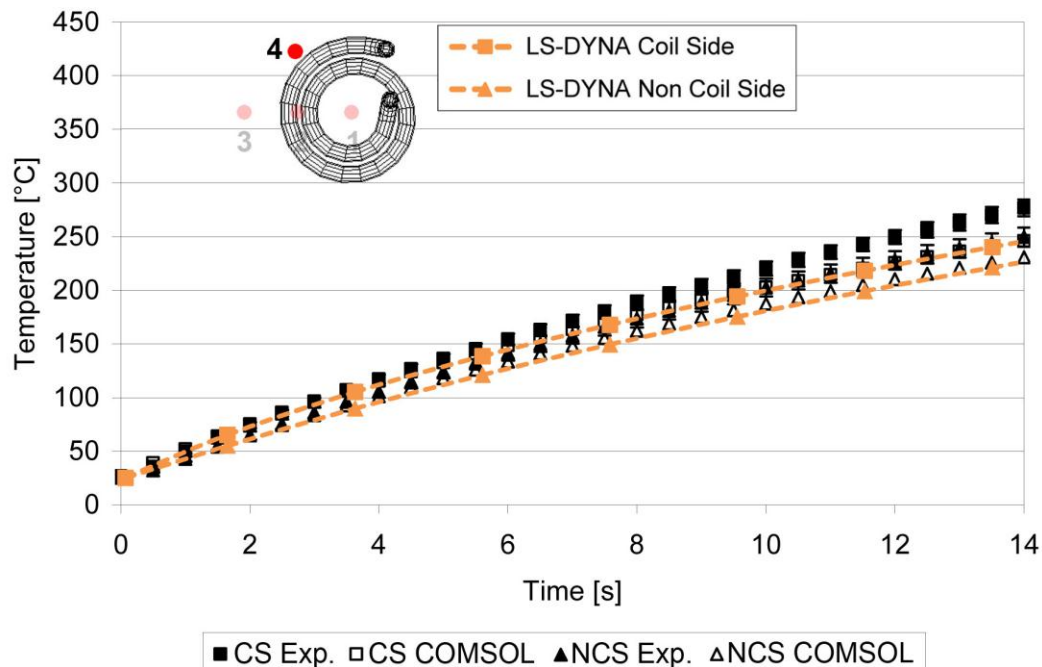


Figure 9: Comparison of a) LS-DYNA and b) COMSOL thermal contour plots in °C for a structural steel plate at 10% (131.97A) power and a coupling distance of 2mm, frequency 400 kHz.

4-3-2 CF/PEEK Composite plate

The same study has been performed with a 2 mm thick CF/PEEK composite plate which has an electrical conductivity several orders of magnitude lower than that of structural steel. The graphs in Figures 10 a), b) and c) show the predicted temperature versus time curves at position 4 on the coil-side (CS) and non-coil side (NCS) of the plate specimen for 10, 20, and 30% power and a working frequency of 400 kHz. The temperature sensor location is an arbitrarily chosen point located 10 mm from the center of the coil in the x and y directions. As in one of the steel plate experiments, a constant coupling distance of 2 mm was used.



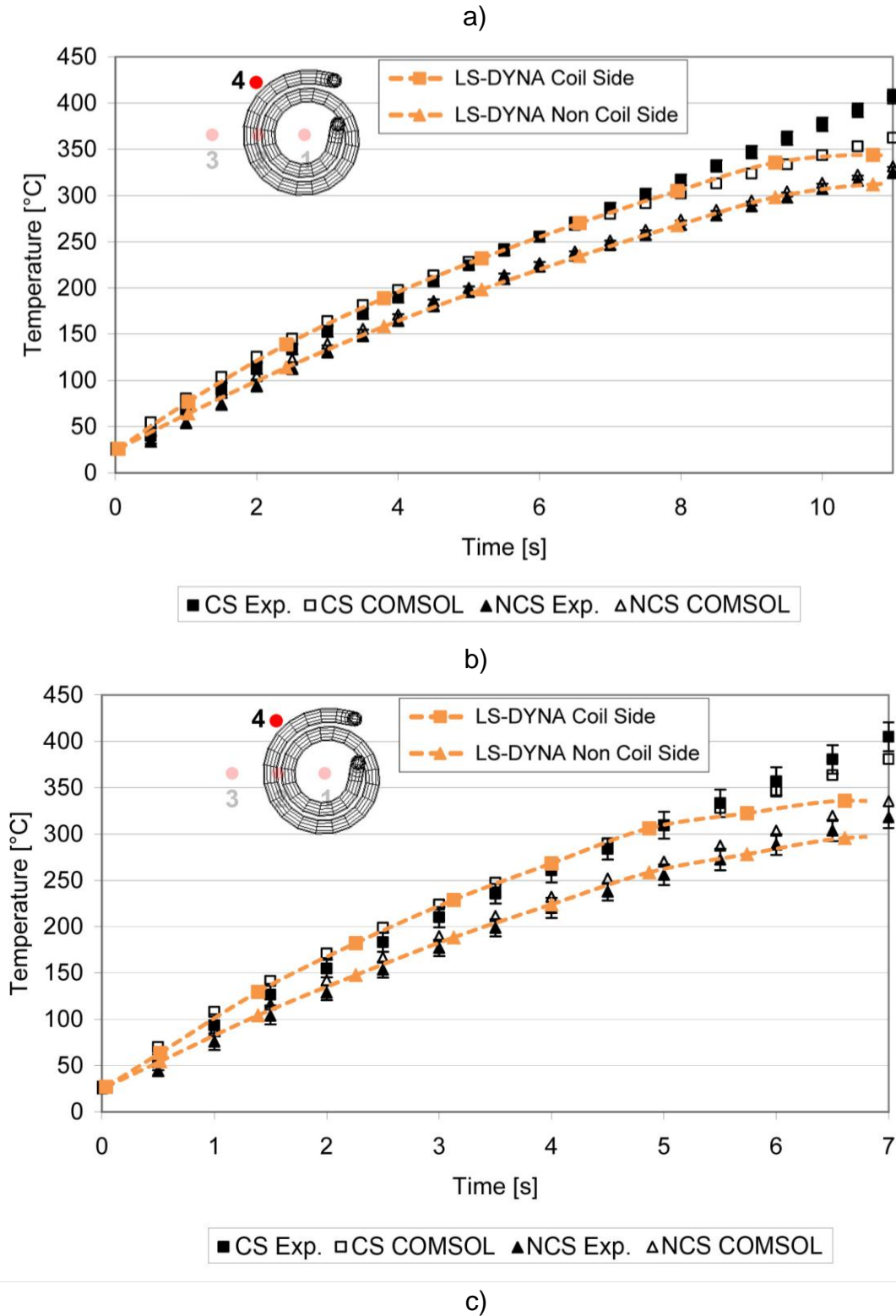


Figure 10: Comparison of LS-DYNA and COMSOL point temperature measurements thermal in °C for a CF/PEEK composite plate at 10, 20 and 30% (131.97A, 193.50 A, 241.54 A) at a coupling distance of 2mm, frequency 400 kHz.

5- Mesh convergence analysis with LS-DYNA

5-1 The model

To perform the convergence analysis a fully meshed pancake coil and steel plate geometry (0.8 mm thick) and the appropriate thermal properties are used. The mesh parameters studied include the number of elements in the thickness dimension of the plate which will be the reference mesh size parameter since the correct representation of the diffusion of the fields in the thickness of the plate will be the leading factor influencing the results. Consistently, the mesh in the thickness of the plate will in every case be 8 times finer than in the plane directions. The mesh sizes studied are: 2, 4, 8 and 16 elements in the plate thickness. The varying parameter for each mesh will be the electrical conductivity since the conductivity has an influence on the skin depth (the bigger the conductivity, the smaller the skin depth). It is interesting to see how the solver reacts when the mesh size is smaller or bigger than the skin depth (Note that in the Eddy current approximation, the EM fields diffuse exponentially through the skin depth). Another parameter that could be varied in future analyses could be the magnetic permeability via the “murel” parameter on the EM_MAT card. Table 2 shows the skin depth calculated by the code for various values of electrical conductivity at 30% power, 2mm coil coupling distance and 400 kHz.

Table 2: Skin depths calculated for different values of electrical conductivity in LS-DYNA

Conductivity (S/m)	Skin Depth (mm)
1e4	8
1e5	2.5
1e6	0.8
1e7	0.25

The extracted variable in this case is the maximum temperature developed in the plate after 20 seconds heating time. It must also be noted that the stability of the EM micro time step varies with the mesh size and the conductivity. For the following analysis, the time step has therefore been adjusted for every case to ensure the convergence of the EM-BEM system.

5-2 Results and observations

Figure 11 shows the behavior of the maximum temperature in the plate versus conductivity for every given element size. It can be observed that the maximum temperature value always increases as the mesh becomes finer. Moreover, in all cases, the maximum temperature starts by going up when the conductivity rises, then reaches a peak and finally decreases when the conductivity keeps increasing. This is consistent with the fact that the Joule heating increases as $\frac{j^2}{\sigma}$. At high conductivity, the current density j is high, but so is the conductivity σ and there is not much Joule heating. If the plate were a perfect conductor, there

would not be any heating at all. At low conductivity, σ is low which makes the Joule heating efficient for a given current density, but j is also low because the coupling between the coil and the plate is low. Again, for a perfect insulator, there would be no heating because no current would be flowing in the plate. Somewhere in between lays therefore a maximum point.

In order to determine if mesh convergence was achieved, we first start by calculating the relative error each time the mesh is refined i.e. the error between two consecutive mesh sizes. We consider that convergence is achieved when the relative error between two consecutive mesh sizes is less than 1%. We see that for the case $\sigma = 1e4 S.m^{-1}$, this is achieved between 4 and 8 elements in the plate thickness. We therefore consider it unnecessary to calculate the 16 elements case where the error would most likely be negligible and therefore we use the 8 elements case as reference for $\sigma = 1e4 S.m^{-1}$. On the other hand, for $\sigma = 1e7 S.m^{-1}$, the relative error between 8 elements and 16 elements is 1.4% which is still higher than 1%. However, as the computer time cost was found to significantly increase with a finer mesh, it was decided to use the 16 element value as a reference value for $\sigma = 1e7 S.m^{-1}$ keeping in mind that the true converged value is probably slightly higher.

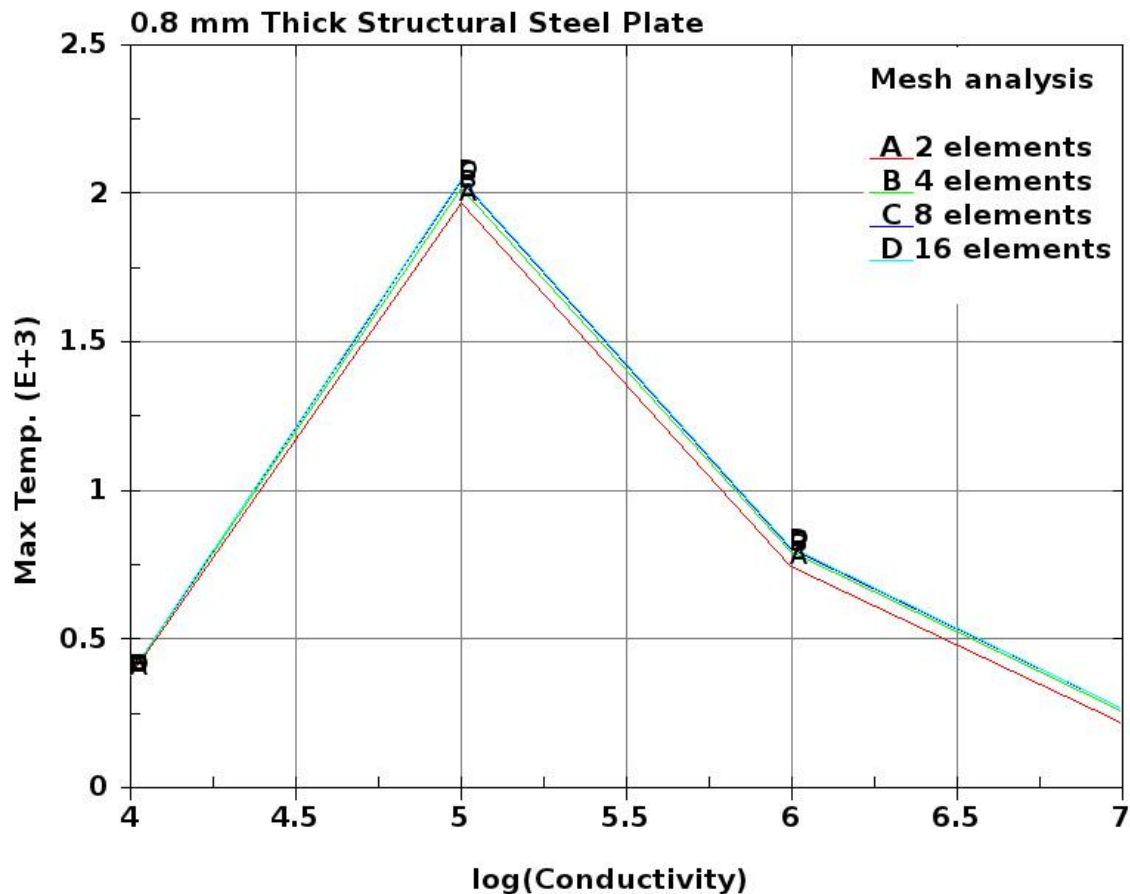


Figure 11: Graphical representation of the maximum temperature developed after 20 seconds in a 0.8 mm thick plate for different values of electrical conductivity using different through thickness mesh resolutions

Now, that the reference values have been established, we can calculate the absolute error which shows the error between a given value and the reference value. Figure 12 shows how this absolute error behaves as a function of the mesh size for four conductivity values. It can be seen that the absolute error increases with the conductivity as well as with the coarseness of the mesh. While looking at Table 2, it can be noted that for the coarsest mesh and $\sigma = 1e7 \text{ S.m}^{-1}$, where the absolute error is at its highest point, there is less than 1 element in the skin depth.

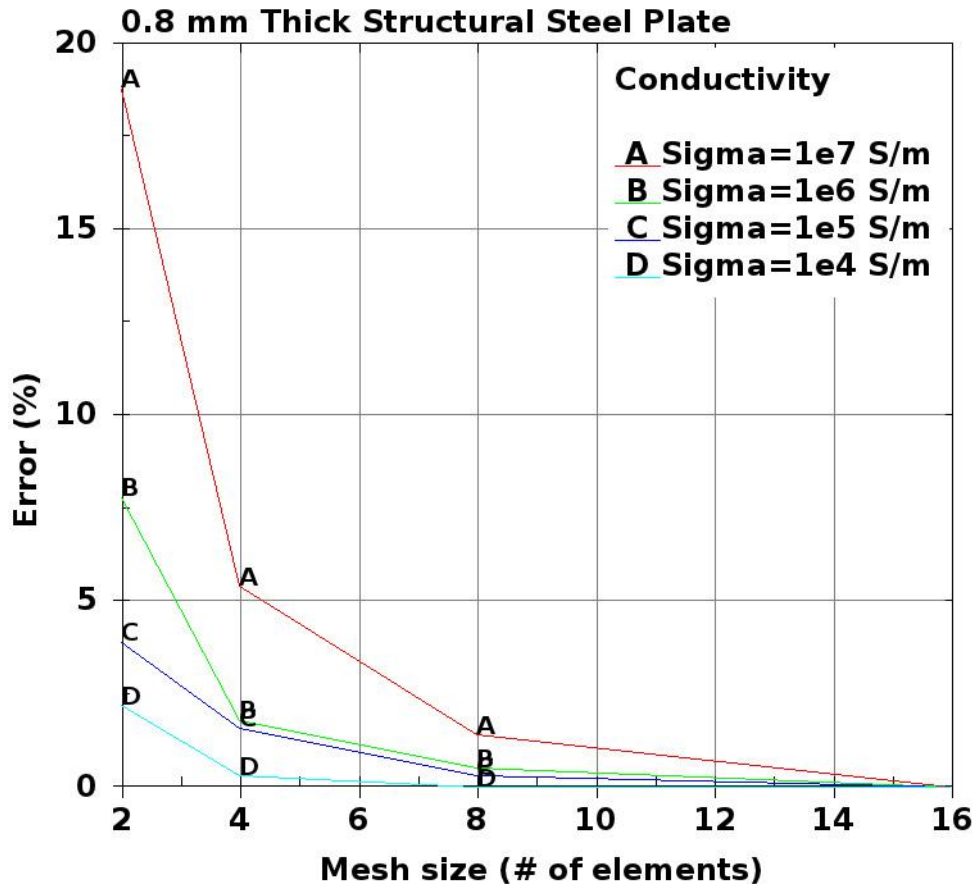


Figure 12: Absolute error (%) in the maximum plate temperature after 20 second's heating with respect to the through thickness mesh size for different electrical conductivity values

Let us now introduce Table 3 that sums up the results that have been obtained. For every case, the temperature as well as the absolute and relative error is given. However, the main mesh parameter will now be the number of elements through the skin depth instead of the number of elements in the thickness. This way, the results appear in a new light since the effect of the conductivity can clearly be seen and a number of conclusions can be drawn. It indeed appears that the more elements we have in the skin depth, the more accurate the results. It explains why for the $\sigma = 1e4 \text{ S.m}^{-1}$, the results appear already very accurate with a coarse mesh as there are already 20 elements in the skin depth. On the other hand, with less than 1 element for $\sigma = 1e7 \text{ S.m}^{-1}$, the error is big but rapidly decreases as soon as there is more than one element in the skin depth.

Table 3: Relative and Absolute error calculation for different electrical conductivity values and therefore skin depths with respect to chosen element size

Conductivity	1e4	1e5	1e6	1e7
$\frac{\Delta SkinDepth}{\Delta EleSize}$	20	6.25	2	0.625
Max Temperature (Absolute Error) (Relative Error)	375.3 (2.5%) (2.2%)	1970 (3.9%) (2.3%)	745.6 (7.8%) (6.1%)	220 (18.8%) (14.1%)
$\frac{\Delta SkinDepth}{\Delta EleSize}$	40	12.5	4	1.25
Max Temperature (Absolute Error) (Relative Error)	383.8 (0.3%) (0.3%)	2017 (1.6%) (1.3%)	793.7 (1.8%) (1.3%)	256.2 (5.4%) (4.0%)
$\frac{\Delta SkinDepth}{\Delta EleSize}$	80	25	8	2.5
Max Temperature (Absolute Error) (Relative Error)	385 (RefValue) (LastValue)	2044 (0.3%) (0.3%)	804 (0.5%) (0.5%)	267 (1.4%) (1.4%)
$\frac{\Delta SkinDepth}{\Delta EleSize}$	160	50	16	5
Max Temperature (Absolute Error) (Relative Error)	-	2050 (RefValue) (LastValue)	808.3 (RefValue) (LastValue)	270.8 (RefValue) (LastValue)

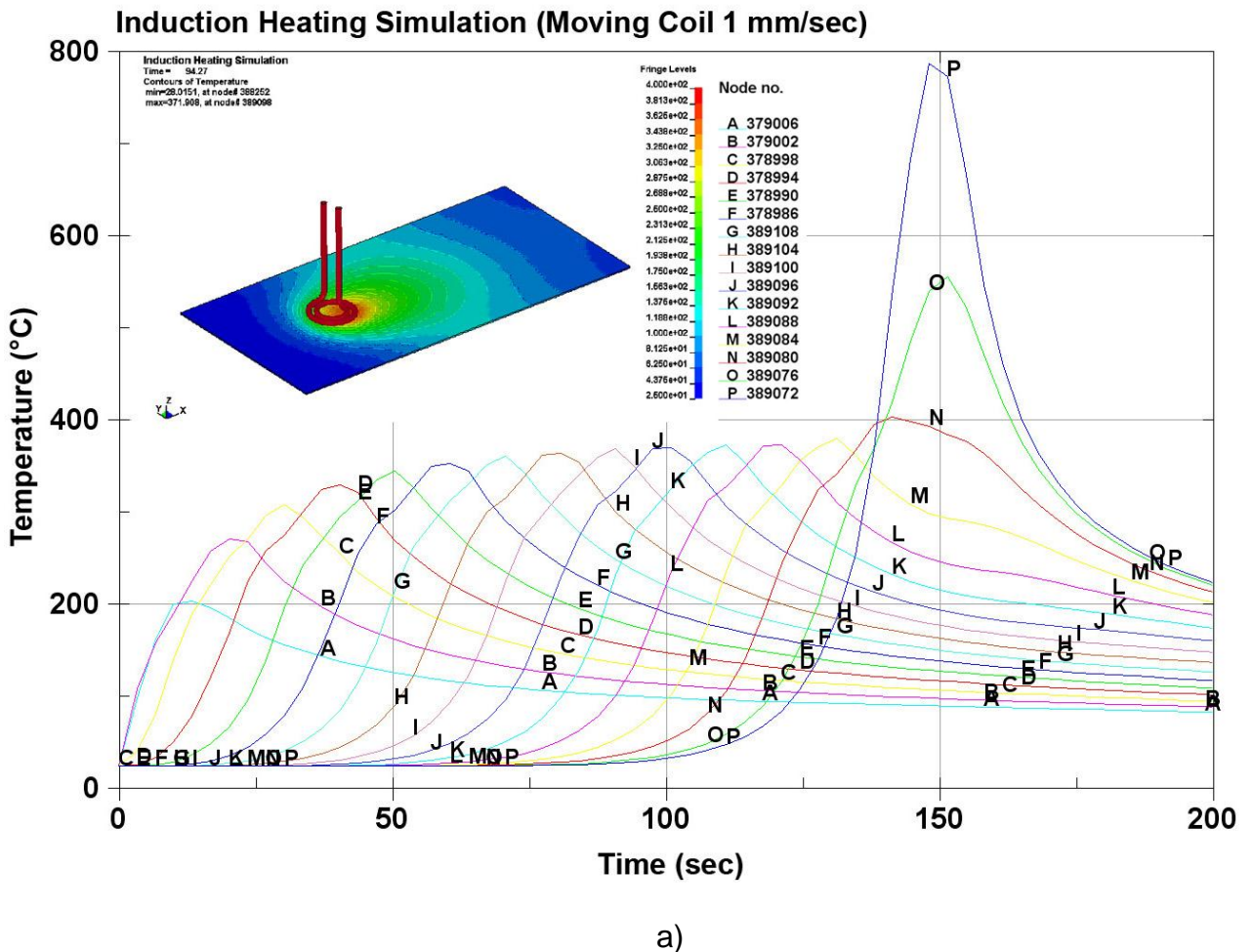
In summary, from Table 3 it can be determined that:

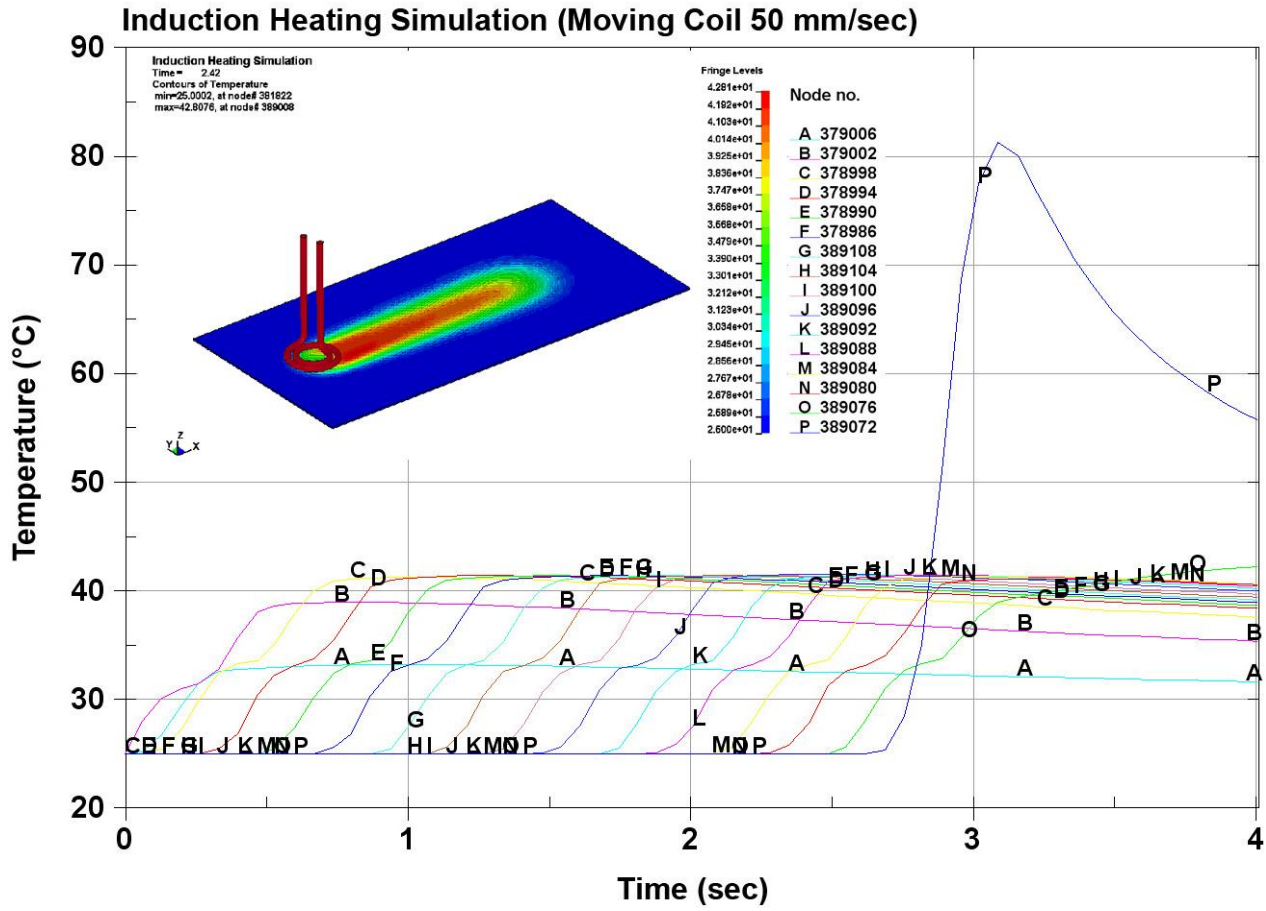
- *With less than one element in the skin depth the error is > 10 %.*
- *Between 1 and 2 elements in the skin depth gives 5 % < Error < 10 %.*
- *For more than 2 elements in the skin depth gives an Error < 5 %.*

This mesh convergence analysis and the resulting table (see Table 3) will therefore be very useful for future analyses. The user can now anticipate the numerical error due to the mesh size relative to the skin depth. It could also be used in order to predict errors when for computer cost reasons, it is impractical to run the case with the fully converged mesh size. For instance, in the $\sigma = 1e7 \text{ S.m}^{-1}$ case, the 16 elements through thickness case has 5 elements in the skin depth. When looking at some other results, it can be assumed that the error between this value and the fully converged value would be between 1.8% (4 elements for $\sigma = 1e6 \text{ S.m}^{-1}$) and 3.9% (6 elements for $\sigma = 1e5 \text{ S.m}^{-1}$).

6-Future analyses with LS-DYNA

One of the main advantages of the electromagnetic modeling approach taken by LS-DYNA is its potential for the simulation of complex coil movements such as those performed by industrial welding robots. With the appropriate additional motion boundary conditions, the models developed here can also be used to verify the heating behavior of moving induction coils across different material types. In fact, any three dimensional motion of the induction coil within the model space could be defined. The aforementioned capability can be particularly useful when defining the complex movement of a thermoplastic induction welding robot in an automotive car assembly plant as was outlined at the beginning of the paper. A preview of this capability is shown in Figure 13 a) and b) where the pancake coil traverses a 100 mm long 0.8 mm thick steel plate at either 1 or 50 mm/min respectively. The temperature contour plots at the top left of each of the two figures show the dramatic difference in the developed heating pattern. If the temperature time history results in the nodes along the center of the plate in the direction of coil movement are plotted with respect to time, then it can be seen that for different speeds a steady state heating temperature can be achieved for performing a welding, curing or heat treating procedure. It can also be seen that the “edge effect” which occurs when the coil passes over the edge of the plate causing a temperature spike is also predicted.





b)

Figure 13: Joule heating in a 0.8 mm thick steel plate resulting from a coil moving at speeds of 1 mm/sec a) and 50 mm/sec b) as predicted by the LS-DYNA inductive heating solver

7-Conclusions

The following work has demonstrated some of the potential of the new induction heating solver available in LS-DYNA. Comparisons with experimental results and an additional EM capable software code COMSOL have validated a variety of heating predictions that can be made. Special care must be taken to define the correct material properties and in particular the correct through thickness mesh density when dealing with workpiece materials with different electrical conductivities as has been demonstrated in the mesh convergence study. For high electrical conductivity materials a larger number of elements should be used to capture correctly the effect of the skin depth. The BEM-FEM modeling approach taken by LS-DYNA eliminates the need for an air mesh and allows more complex moving coil or workpiece cases to be simulated. A preview of this valuable simulation capability has been demonstrated using the case of simple linear coil motion. The demonstrated EM module is integrated into the 980 version of LS-DYNA, which should be released sometime soon. In the meantime, it is available as a “beta version”.

References

- [1] LS-DYNA Theory Manual, LSTC.
- [2] *P. L'Eplattenier, G. Cook, C. Ashcraft, M. Burger, A. Shapiro, G. Daehn, M. Seith*, "Introduction of an Electromagnetism Module in LS-DYNA for Coupled Mechanical-Thermal-Electromagnetic Simulations", 9th International LS-DYNA Users conference", Dearborn, Michigan, June 2005.
- [3] *P. L'Eplattenier, G. Cook, C. Ashcraft* , "Introduction of an Electromagnetism Module in LS-DYNA for Coupled Mechanical-Thermal-Electromagnetic Simulations", Internatinal Conference On High Speed Forming 08, March 11-12, 2008, Dortmund, Germany.
- [4] University of Manchester Structural Fire Engineering Website, <http://www.mace.manchester.ac.uk/project/research/structures/strucfire/materialInFire/Steel/HotRolledCarbonSteel/thermalProperties.htm>, accessed on 10/04/12.
- [5] *V. Kodur, M. Dwaikat, R. Fike*, "High-Temperature Properties of Steel for Fire Resistance Modeling of Structures", Journal of Materials in Civil Engineering, 2010, p 433-434.
- [6] *S. Yafei, N. Dongjie, S. Jing*, "Temperature and Carbon Content Dependence of Electrical Resistivity of Carbon Steel, ICIEA, IEEE 2009, p 368-372.
- [7] *S. Sgobba*, "Physics and Measurements of Magnetic Materials", CERN-2010-004, Geneva, Switzerland, p 39-63.
- [8] *I. Mészáros*, "Testing of Stainless Steel by Double Yoke DC Magnetometer", Journal of Electrical Engineering, Vol 61, No 7/s, 2010, p 62-65.
- [9] *L. Moser, P. Mitschang*, "Experimental Analysis and Modeling of Susceptorless Induction Welding of High Performance Thermoplastic Polymer Composites, Institute für Verbundwerkstoffe GmbH, Kaiserslautern, Germany, 2012.
- [10] Fluxtrol Website, <http://www.fluxtrol.com/products/product-types/fluxtrol-50/>, accessed on 10/04/12.

